Figure S1 related to Figure 1

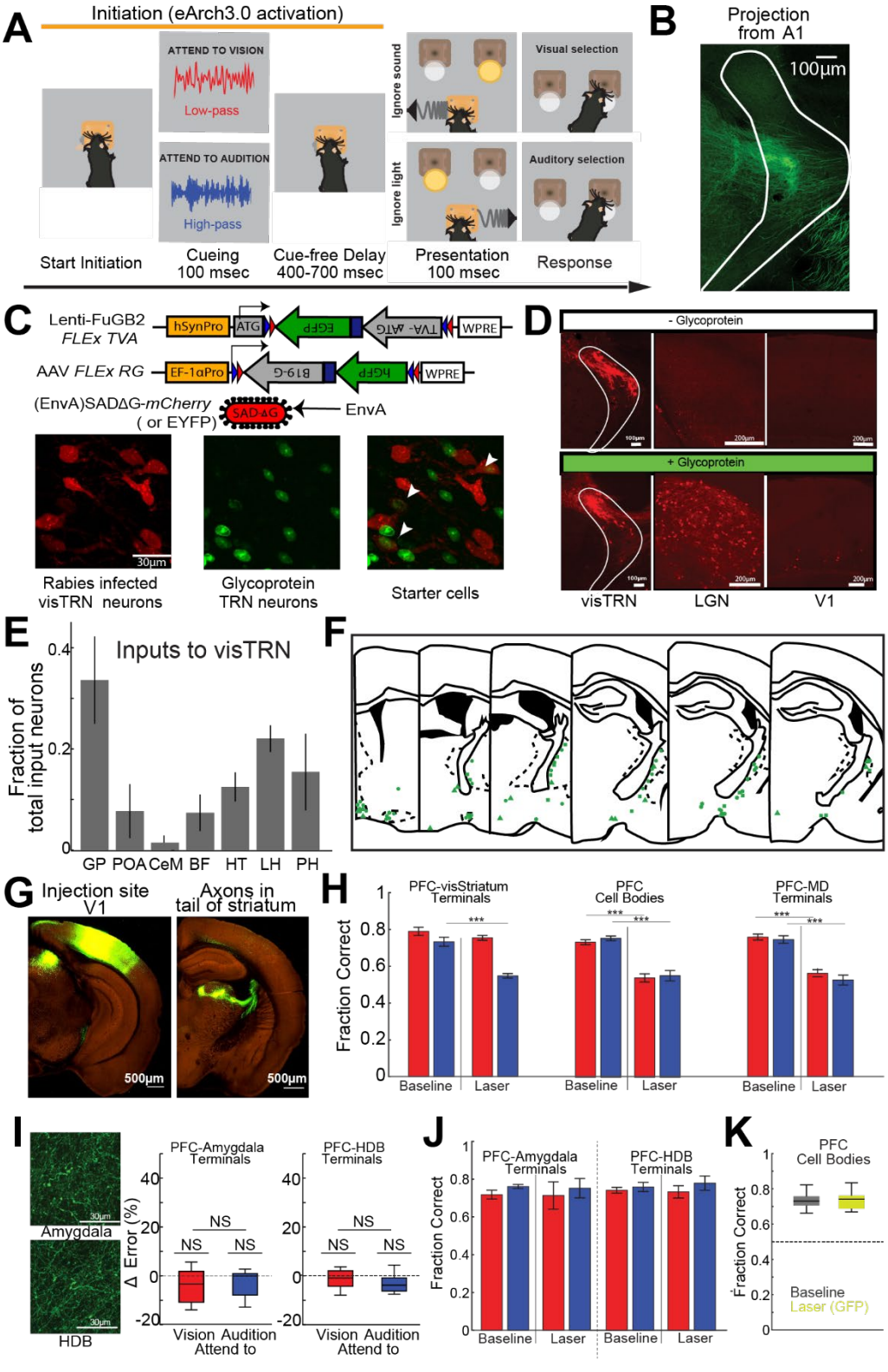

Figure S1: Identification of a behaviorally relevant pathway connecting the PFC to sensory TRN, Related to Fig. 1

A. Detailed schematic of the cross-modal sensory selection task. All the eArch3.0 activation was performed during the initiation (throughout the cuing and cue-free delay; Yellow bar). **B.** Maximal projection confocal images of the presumed location of audTRN showing axons labelled by AAV expressing ChR2-EYFP injected in the auditory cortex (A1). Putative audTRN receives projections from auditory cortices. **C.** (Top)Two helper virus gene cassettes used to express either Cre-dependent TVA-mCherry or rabies glycoprotein and a cartoon of EnvA-pseudotyped, glycoprotein deleted rabies viruses (RVΔ*G*). (Bottom) Maximal projection confocal images of starter cells in visTRN. Neurons expressing both RVΔ*G* (infected visTRN neurons, red, left), rabies glycoprotein (TRN neurons, green, center) are potential starter cells of monosynaptic regrade tracing (arrowhead, right). **D.** (Top) In the absence of rabies glycoprotein the rabies virus infect only visTRN neurons (left) but didn't not retrogradely label visual thalamus (LGN, middle) or visual cortex (V1, right) (Bottom) When visTRN also expressed rabies glycoprotein, visTRN neurons and known inputs to visTRN were successfully labeled with mCherry (red, visTRN-left, LGN-middle, V1-right) indicating that RVΔG successfully labeled presynaptic neurons of visTRN. **E.** Summary of input neurons (excluding thalamus/cortex/midbrain) to visTRN ($p = 0.0027$ Main Effect of brain region kruskal-wallis ANOVA, N = 5 mice) showing that major inputs to visTRN are GP. GP, globus pallidus; POA, the preoptic area; CeM, the medial part of central amygdala; BF, basal forebrain; HT, medial hypothalamus; LH, lateral hypothalamus; PH, posterior hypothalamus. **F.** Cartoon showing the location of rabies infected input neurons to visTRN (excluding thalamus/cortex/midbrain). **G.** Reproduction of projection experiment data (© 2011 Allen Institute for Brain Science. Allen Mouse Brain Connectivity Atlas. Available from: (http://connectivity.brain-map.org/projection/) with eGFP injections into either visual cortex (experiment 113887162) and serial two-photon tomography showing innervation to the visStriatum (Oh et al., 2014). **H.** Task performances for each trial type (Red: attend to vision, Blue: attend to audition) on cross-modal sensory selection task without (Baseline) or with optogenetic manipulation (Laser). Optogenetic manipulations were performed in the following regions: (Left) PFC terminals in visStriatum (Middle) PFC cell bodies (Right) PFC terminals in MD. **I.** (Left) Maximal projections of PFC terminal confocal images in the amygdala (top) or HDB (bottom). No behavioral changes were observed in the cross-modal sensory selection task with PFC terminal suppression in either structure (*attend to vision* trials-red, *attend to audition* trials-blue) (N = 5 mice, n = 20 sessions). **J.** Task performances for each trial type (Red: attend to vision, Blue: attend to audition) on cross-modal sensory selection task without (Baseline) or with optogenetic manipulation (Laser). Optogenetic manipulations were performed in the following regions: (Left) PFC terminals in Amygdala ies (Right) PFC terminals in HDB. **K.** Laser stimulation of GFP expressing PFC neurons did not affect the task performance. No significant behavioral changes were observed if GFP was expressed instead of eArch3.0. (n=4 mice, 18 sessions, sign-rank test).

Boxplots: median (line), quartiles (box), 95% confidence interval (whiskers)

Figure S2 related to Figure 3

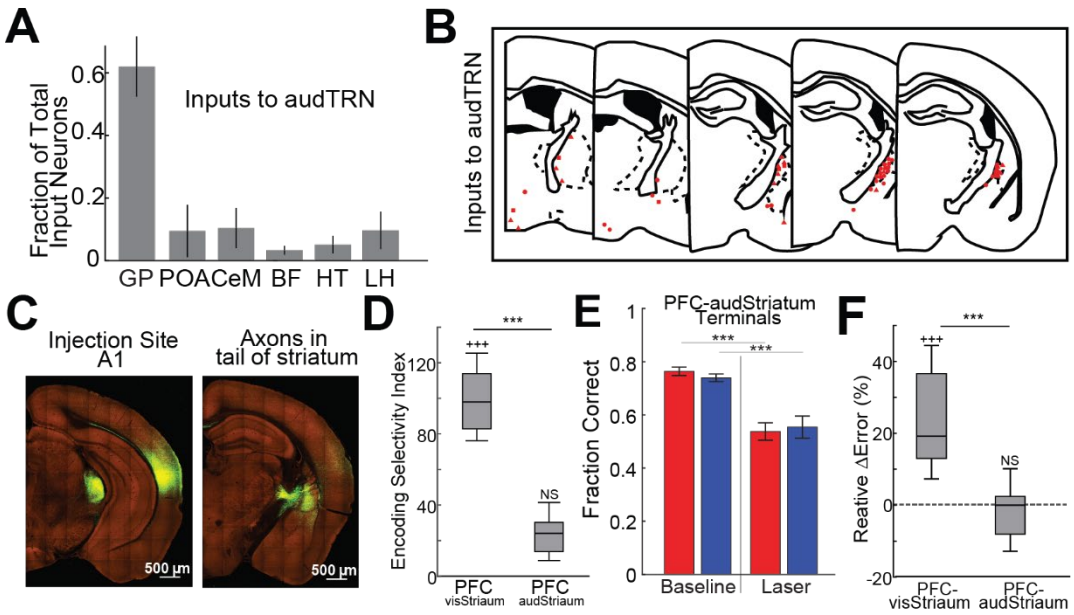

Figure S2: Assessment of pathway connecting PFC to audTRN, Related to Fig. 3

A. Summary of input neurons (excluding thalamus/cortex/midbrain) to audTRN neurons (p = 0.005 Main Effect of brain region kruskal-wallis ANOVA, N = 5 mice) showing GP inputs to audTRN neurons. GP. GP, globus pallidus; POA, the preoptic area; CeM, the medial part of central amygdala; BF, basal forebrain; HT, medial hypothalamus; LH, lateral hypothalamus. **B.** Cartoon showing the location of rabies infected input neurons to audTRN (excluding thalamus/cortex/midbrain). **C.** Reproduction of projection experiment data (© 2011 Allen Institute for Brain Science. Allen Mouse Brain Connectivity Atlas. Available from: (http://connectivity,brain-map.org/projection/) with eGFP injections into auditory cortex (experiment 112881858), and serial two-photon tomography showing innervation in the striatum (Oh et al., 2014). **D.** Quantification of the relative selectivity in cue encoding comparing $PFC_{visStriatum}$ and $PFC_{audstriatum}$ population. Selectivity was estimated by taking the difference in decoding accuracy above chance between the two cue types and normalizing it to the average decoding accuracy for the preferred cue type. The selectivity of the $PFC_{visStriatum}$ population was significantly greater than that of the $PFC_{audstriatum}$ population consistent with the idea that $PFC_{audstriatum}$ neurons are engaged for both '*attend to vision*' and '*attend to audition*' trials (N = 5 mice, n = 1441 neurons; *** p<0.001, pairwise rank-sum test; +++ p<0.001, vs baseline). **E.** Task performances for each trial type (Red: attend to vision, Blue: attend to audition) on cross-modal sensory selection task without (baseline) or with optogenetic manipulation (laser). Optogenetic manipulations were performed in the following regions: (Left) PFC terminals in audStriatum. **F.** Suppression of PFC-audStriatum terminals showed a smaller difference in behavioral effects across trial types consistent with the idea that, in contrast to the $PFC_{visStriatum}$ output, this output is needed both to broadly suppress audition on '*attend to vision*' trials and to improve auditory discrimination on '*attend to audition*' trials (N = 12 mice, n = 44 sessions; *** p<0.001, pairwise rank-sum test; +++ p<0.001, compared to baseline).

Boxplots: median (line), quartiles (box), 95% confidence interval (whiskers)

Figure S3 related to Figure 4

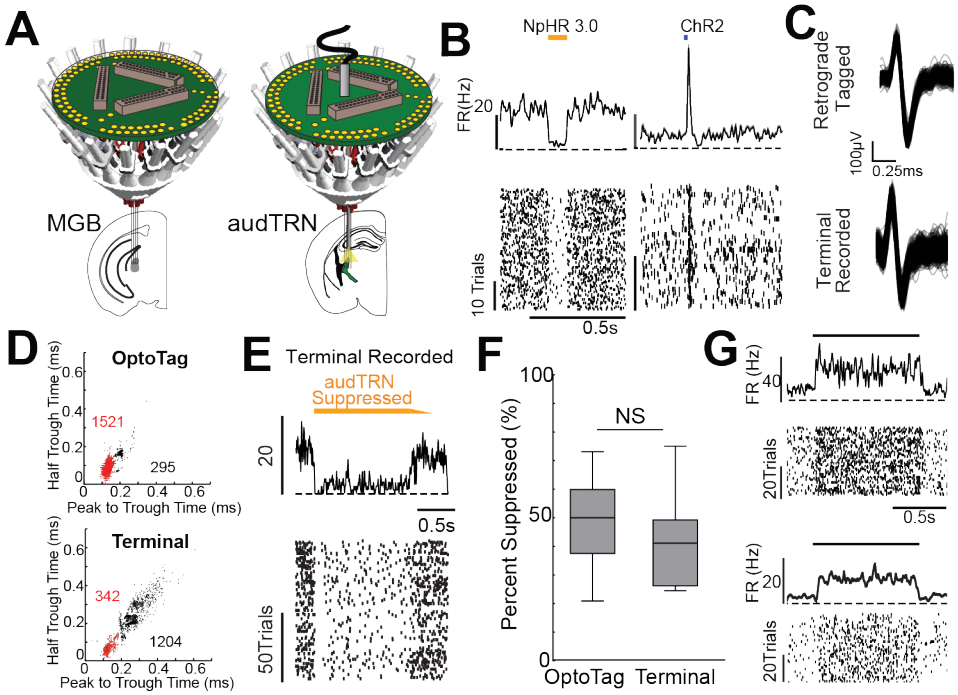

Figure S3: Comparison of audTRN neuron recordings with FS putative audTRN neuron terminals recorded in MGBv, Related to Fig. 4

A. Schematic of multi-electrode drive targeting the MGBv used for recording audTRN terminals in MGBv or retrograde optogenetically tagged audTRN neuron cell bodies within the TRN. **B.** Example PSTHs (top) and rasters (bottom) showing short latency optogenetic suppression (yellow bar) of an audTRN neurons that expressed either eNpHR3.0 (left) or ChR2 (right) respectively. **C.** Comparison of waveforms of directly tagged (top) and MGB terminal recorded (bottom) audTRN neurons. **D.** Plot of waveform properties used to isolate terminal responses of audTRN projections for direct tagged (top) and terminal recorded (bottom) units showing clear cluster separation between fast spiking (FS) audTRN terminal spikes (red) and regular spiking (RS) MGB somatic spikes (audTRN: N = 5 mice, 1816 neurons, MGB: N = 5 mice, 1546 neurons) **E.** Example PSTHs (top) and rasters (bottom) showing an example neuron showing suppression of a waveform identified terminal recording showing suppression by somatic NpHR 3.0 activation in the audTRN. **F.** Boxplot showing the proportion of significantly suppressed (see methods) FS neurons recorded in the TRN (Opto-Tag) or FS neuron terminals recorded in the MGBv (Terminals) across sessions (> 25 sessions per group, > 3 FS neurons per session). A similar number of suppressed neurons were recorded in both structures (audTRN: N = 3 mice, 1089 total neurons, MGB: N = 3 mice, 927 total neurons, pairwise rank-sum test). **G.** Comparison of the responses to sound of directly tagged (top) and MGB terminal recorded (bottom) audTRN neurons. Both neurons showed non-specific increase of spike rates to sound stimuli.

Boxplots: median (line), quartiles (box), 95% confidence interval (whiskers)

Figure S4 related to Figure 5

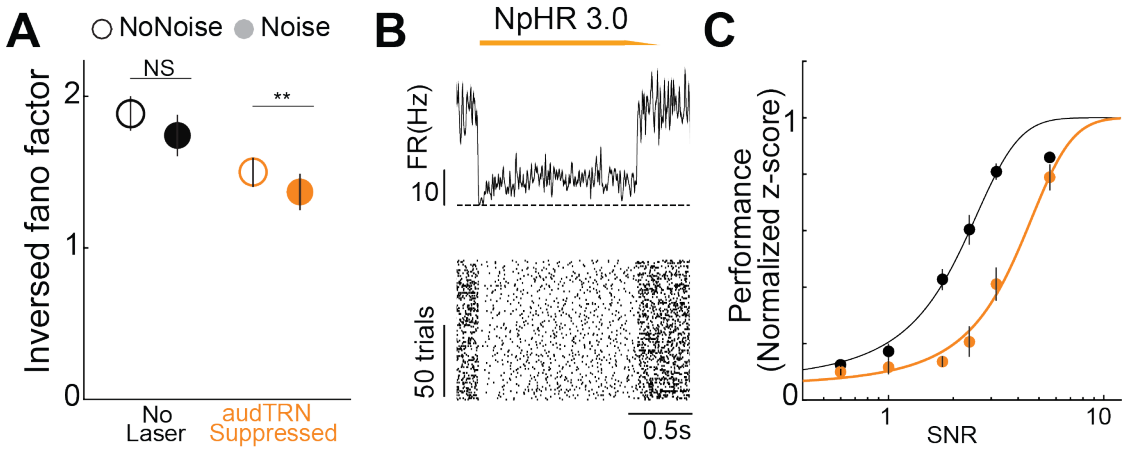

Figure S4: The role of audTRN in enhancing MGBv SNR, Related to Fig. 5

A. Mean and standard error of inverse fano factors estimated across repeated presentations of dynamic random chords (N = 3 mice, n = 430 neurons, **p<0.01, pairwise sign-rank test). **B.** Example PSTH (top) and raster (bottom) from a single audTRN neuron showing the viability of eNpHR 3.0 based suppression of the audTRN. 1.5 s of eNpHR3.0 activation (with ramping offset to prevent rebound responses, yellow bar) successfully suppressed spike rates of audTRN. **C.** Psychometric functions across SNR values for control trials (no laser) in black or audTRN suppressed trials in yellow normalized to the maximum performance level showing the remaining shift in discrimination threshold.

Figure S5 related to Figure 7

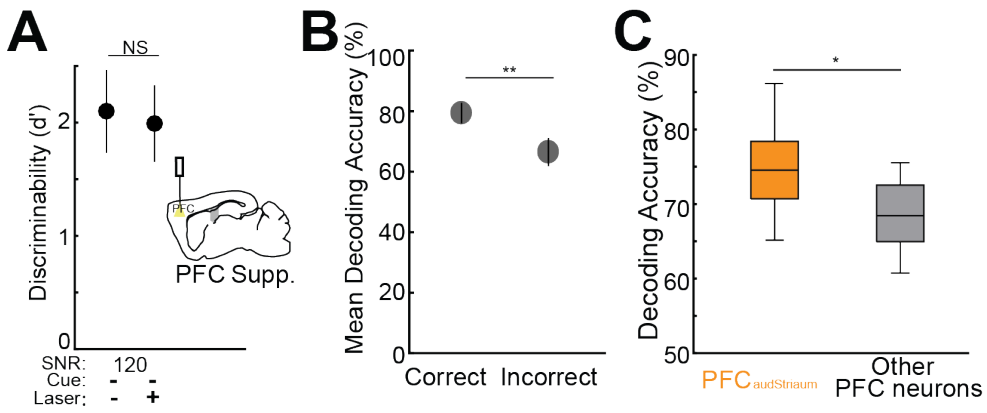

Figure S5: PFC engagement is not necessary for performance of auditory discrimination task but lower engagement is associated with incorrect responses on noise trials, Related to Fig. 7

A. There was no effect of PFC suppression (Laser) on no noise trials (SNR = 120; p = 0.23 pairwise rank-sum test, N = 6 mice, n = 6 sessions/mouse/condition). **B.** Comparison of decoding accuracy for correct and incorrect trial sets in which predictive cue was presented. Incorrect trials showed a reduction in effective encoding of the predictive cue (N = 4 mice, n = 863 neurons, * p < 0.05 rank-sum test) consistent with the idea that cue encoding was beneficial for task performance. **C.** The predictive cue was much more decodable from the $PFC_{audStriatum}$ neurons, compared with the one of other PFC neurons (N = 4 mice, n = 112 tagged, 751 nontagged neurons, * p < 0.05 rank-sum test).